Improvement of Wave Boundary Layer Theory Applied in Atmosphere-Wave Coupled Model

Ting Zhang[1]

[1]Zhejiang University

November 21, 2022

Abstract

The wave boundary layer (WBL) theory from low to extreme winds is improved based on the governing equations of airflow with suspended spray droplets. The modified theory accounts for the vertical variation of turbulent momentum fluxes and gives the explicit solution of mean wind profiles in the WBL. Applying the traditional and modified WBL theories into the numerical atmosphere-wave coupled model respectively, one-dimensional experiments are conducted to investigate the impact of surface waves and ocean spray on air-sea momentum fluxes. It's found the simulated momentum flux according to the modified WBL theory could better explain the distribution of field observational data, particularly under high winds. The simulated results also reveal wave fields become younger with increasing wind speed when the modified WBL theory is adopted. Moreover, the research results motivate the application of the WBL theory in earth system models.

Improvement of Wave Boundary Layer Theory Applied in Atmosphere-Wave Coupled Model

Ting Zhang[1,2]

[1]Ocean College, Zhejiang University, Zhoushan, P.R. China
[2]Department of Earth Sciences, Uppsala University, Uppsala, Sweden

Key Points:

- A wave boundary layer (WBL) theory from low to extreme winds is improved.
- The theory considers the vertical variation of turbulent momentum fluxes in the WBL.
- The WBL theory is applied into the numerical atmosphere-wave coupled model to conduct one-dimensional simulations.

Corresponding author: Ting Zhang, zhangting_emmas@163.com

Abstract

The wave boundary layer (WBL) theory from low to extreme winds is improved based on the governing equations of airflow with suspended spray droplets. The modified theory accounts for the vertical variation of momentum fluxes and gives the explicit solution of mean wind profiles in the WBL. Applying the traditional and modified WBL theories into the numerical atmosphere-wave coupled model respectively, one-dimensional experiments are conducted to investigate the impact of surface waves and ocean spray on air-sea momentum fluxes. It's found the simulated momentum flux according to the modified WBL theory could better agree with the field observational data, particularly under high winds. The simulated results also reveal wave fields become younger with increasing wind speed when the modified WBL theory is adopted. Moreover, the research results motivate the application of the WBL theory in earth system models.

Plain Language Summary

Ocean surface is covered with surface waves which significantly participate in air-sea interaction process. Hence, the lowest 10 m above mean sea surface is generally called wave boundary layer (WBL). The physical progress in the WBL becomes complicated In conditions of high winds. Following the intensive wave breaking and related phenomena, such as foam coverage and bubble bursts, numerous small water droplets are ejected from sea surface. These spray droplets mainly influence the momentum exchange in the WBL. Therefore, a theory which can parameterize the impact of surface waves and ocean spray on the WBL is necessary to improve the coupled atmosphere-ocean models. Present study tries to improve the current WBL theory to make it more available for various situations occurred in the WBL.

1 Introduction

Investigation of the air-sea momentum flux (wind stress or drag coefficient) from low to extreme winds is one of the most significant subjects in modeling meteorological and oceanographic processes. However, the development in parameterizations of air-sea fluxes remains limited due to the lack of accurate understanding air-sea interaction in the wave boundary layer (WBL), particularly under extreme winds (Powell et al., 2003; Donelan et al., 2004; Jarosz et al., 2007).

Surface waves are responsible for the momentum transfer in the WBL (Hara & Belcher, 2004; Kudryavtsev et al., 2014; Wu et al., 2017). Under high wind conditions, suspended spray droplets also exchange momentum with their ambient airflow before falling back to sea surface (Andreas, 2004; Wu et al., 2015; Zhang et al., 2016). In many numerical atmospheric models, wind stress is parameterized through the bulk formula in which the roughness length of sea surface is related to both surface wave and spray droplets. There are various parameterizations on the roughness length, such as depending on wave ages or wave steepness (Stewart, 1974; Taylor & Yelland, 2001; Liu et al., 2012). The most classical is the Charnock relation, i.e., $z_0 = \alpha u_*^2/g$, where α is the Charnock coefficient, u_* is the friction velocity and g is the gravitational acceleration. Some studies pointed out the Charnock coefficient should be a constant ranging from 0.01 to 0.03 regardless of wave state whereas some others addressed it should depend on wave waves or the combination of wave ages and spray droplet concentration (Drennan et al., 2003; Moon et al., 2004; Zweers et al., 2015).

Considering surface waves participate in the distribution of momentum fluxes in the WBL, Janssen (1991) initially parameterized the Charnock coefficient through the wave-induced stress. Applying this theory to the wave model coupled with a simple surface-layer model, the simulation results plausible explained the experimental drag coefficients observed on the North Sea. Afterwards, this approach to parameterize Charnock coefficient is implemented into the third-generation wave model, i.e., WAVEWATCH III. Although the model could directly compute the momentum supported by surface waves, it failed to simulate the drag coefficient to match the observations at high winds. One possible reason owns to the neglect of spray impact on the WBL.

Based on the classical theory on the motion of suspended droplets in the airflow, Kudryavtsev and Makin (2011) introduced a volume source of spray droplets to the governing equations for the WBL. The spray impact on the momentum flux are discussed in their study whereas they took no consideration of wave impact on the WBL. Furthermore, Zhang and Song (2018) considered the wave-induced stress into the theoretical model of Kudryavtsev and Makin (2011) to investigate the combined effects of surface waves and spray droplets on the WBL. They found wave-induced stress only influences the drag coefficient at low-to-moderate winds and it could be negligible in comparison with the spray-induced stress under high winds. The spray-induced stress in their studies might be exaggerated due to the introduction of the spray volume source. Correspondingly, the wave-induced stress might be underestimated so that the wave impact on momentum flux is ignored.

Considering surface waves and ocean spray are main quantities controlling momentum transfer in the WBL. The objective of this study is to improve the WBL theory applicable from low to high winds. Then this theory is applied to the numerical atmosphere-wave coupled model and one-dimensional simulations are conducted. The rest of this paper is organized as follows. Section 2 proposes the improved WBL theory applicable from low to extreme winds. It is the extension of the theory on the motion of suspended droplets. Section 3 gives a description of the atmosphere-wave coupled model, including the WBL theory it currently adopts, model components and coupling fields. Section 4 illustrates how the modified WBL theory is applied to the atmosphere-wave coupled system. The one-dimensional simulations are presented in section 5, including experiment designs and analysis of the simulation results. Conclusion and discussion are given in section 6.

2 Improved WBL theory

Ocean spray gradually generate as wind approaching hurricane strength in the WBL. Herewith, the suspended spray droplets should be considered in the conservation equations of the mass and momentum above surface waves. Based on the theory of suspended motion in the airflow (Barenblatt, 1953), five postulations are suggested here: (i) the in-compressible airflow with suspended spray droplets is stationary and horizontally homogeneous; (ii) the sizes of suspended spray droplets are small in comparison with those of turbulence length scales; (iii) the horizontal velocities of the airflow and spray droplets are same whereas their vertical velocities differ by the terminal velocity of spray droplets; (iv) the mean concentration of spray droplets is small; (v) some part of momentum are transported from airflow to the surface waves which align to the mean airflow direction. Based on the assumptions above, the momentum conservation equation for the airflow in the WBL is written as (the detailed derivation is shown in Appendix),

$$\frac{\partial}{\partial z}\left(\overline{\widetilde{U}\widetilde{w}} + \overline{U'w'} - \frac{\rho_w}{\rho}\overline{U's'a}\right) = 0 \ , \tag{1}$$

where ρ is the density of the mixture defined as the airflow containing spray droplets; U' and $\widetilde{U}$ respectively denote turbulent and spray-induced fluctuations in the horizontal velocity of airflow; w' and $\widetilde{w}$ respectively denote turbulent and wave-induced fluctuations in the vertical velocity of airflow; s' is the spray concentration; a is the mean fall velocity of spray droplets; and the overbars denote time averaging.

Integrating Eq. (1) from the local altitude z to the place h where the impact of surface waves and spray droplets on the WBL disappears, Eq. (1) becomes

$$\rho\overline{U'w'}|_{z=h} - \left(\rho\overline{\widetilde{U}\widetilde{w}} + \rho\overline{U'w'} - \rho_w\overline{U's'a}\right)|_z = 0 \ . \tag{2}$$

According to the definition of turbulent and wave-induced stress (Makin & Mastenbroek, 1996), i.e., $\tau_t = -\rho\overline{U'w'}$ and $\tau_w = -\rho\overline{\widetilde{U}\widetilde{w}}$, Eq. (2) is rewritten as

$$-\rho_a u_{*h}^2 + \tau_w(z) + \tau_t(z) + \rho_w\overline{U's'a}|_z = 0 \ , \tag{3}$$

where u_{*h} is the friction velocity outside the layer affected by surface waves and ocean spray, i.e., $u_{*h} = \sqrt{\tau_t(h)/\rho_a}$. The last term on the left-hand side of Eq. (3) parameterizes the momentum transfer between the airflow and spray droplets. It is defined as the spray-induced stress here, i.e., $-\rho_w\overline{U's'a} = \tau_{sp}$. Thus, Eq. (3) is equivalent to

$$\tau_t(z) = \rho_a \times u_{*h}^2 - \tau_w(z) + \tau_{sp}(z) \ , \tag{4}$$

which implies the turbulent stress in the layer influenced by waves and droplets varies with height. Correspondingly, the friction velocity $u_*(= \sqrt{\tau_t(z)/\rho})$ also changes with height rather than retaining constant.

Based on the closure scheme for the turbulent flow, the turbulent stress on the left-hand side of Eq. (4) accords with

$$\tau_t(z) = \rho K\frac{dU(z)}{dz} \ , \tag{5}$$

where K is turbulent eddy viscosity of the mixture. For simplicity, $U(z)$ denotes the mean horizontal velocity of airflow instead of $\overline{U(z)}$. Here, we follow the conclusion of Kudryavtsev and Makin (2011) that spray impact on the WBL stratification is so weaker that the Monin-Obukhov similarity theory for neutral boundary layer could be applied for the airflow with suspended droplets. Hence, the turbulent eddy viscosity is parameterized by the following form

$$K = \kappa z u_*(z) \ , \tag{6}$$

where $\kappa = 0.4$ is the Von *Kármán* constant. Using the closure scheme in Eq. (5), K can be expressed as a function of mean velocity shear of airflow, i.e.,

$$K = \kappa^2 z^2\frac{dU(z)}{dz} \ . \tag{7}$$

Therefore, substituting Eq. (4) into Eq. (5) and integrating Eq. (1) from the aerodynamic roughness length z_0 to z, the mean wind speed in the WBL reads

$$U(z) = \int_{z0}^{z}\frac{\rho_a u_{*h}^2 - \tau_w(z) + \tau_{sp}(z)}{\rho}K^{-1}dz \ , \tag{8}$$

which satisfies the bottom boundary condition, i.e., $U(z_0) = 0$. Equation (8) implies both the wave-induced and spray-induced stress affect the shape of wind profiles in the WBL. It could turn into the logarithmic profile in no consideration of the wave-induced and spray-induced stress, i.e.,

$$U(z) = \frac{u_*}{\kappa}\ln\left(\frac{z}{z_0}\right) \ , \tag{9}$$

which is generally used in coupled or uncoupled atmosphere, wave and ocean numerical models to estimate air-sea momentum fluxes. Equation (9) is also called bulk formulation, which avoids complicated parameterizations of the wave-induced and spray-induced stress in Eq. (8).

3 The Atmosphere-Wave Coupled Model

The Uppsala University Coupled Model (UUCM) is developed at the Meteorology group of Uppsala University. It consists of air-sea, air-wave, air-wave-sea and air-sea-ice coupled models. Present study only adopts one part of this coupled system, including an atmosphere model, i.e., Weather Research Forecasting (WRF) and a third generation wave model, i.e., WAVEWATCH III (WW3). These two components are coupled to each other through OASIS3-MCT coupler. The coupling fields significantly determine air-sea processes in the WBL. The wave model provides the wave information for the atmosphere model. On the other hand, the atmosphere model provides wind forcing to the wave model to generate surface waves.

Currently, the WBL theory of Janssen (1991) is implemented into the coupled system to estimate air-sea momentum fluxes. Assuming mean wind profiles present the logarithmic shape as Eq. (9), a parameter z_1 is introduced to parameterize the impact of gravity-capillary waves, i.e.,

$$U(z) = \frac{u_*}{\kappa} \ln\left(\frac{z+z_1}{z_0+z_1}\right) . \tag{10}$$

The momentum conservation equation at the sea surface reads

$$\tau = \tau_t(z=z_0) + \tau_w(z=z_0) , \tag{11}$$

where $\tau = \rho_a u_*^2$ is defined as the total wind stress in which the friction velocity u_* is constant in the WBL. According to the turbulent closure scheme in Eq. (5), the total wind stress in Eq. (11) is written as

$$\tau_t(z) = \left(\frac{\kappa U(z)}{\ln(z/z_2)}\right) \text{, where } \ z_2 = \alpha\frac{u_*^2}{g} \ , \quad \alpha = \frac{0.001}{\sqrt{1-x}}, \quad x = \frac{\tau_w(z_0)}{\tau} \ . \tag{12}$$

In addition, the drag coefficient C_d defined by the friction velocity u_* and the 10-m wind speed U_{10} is expressed as

$$C_d = \left(\frac{u_*}{U_{10}}\right)^2 = \left(\frac{\kappa}{\ln(10/z_2)}\right)^2 . \tag{13}$$

Herewith, after the coupled system starts up, the wave model regularly transfers the Charnock coefficient α upward to the atmosphere model and receives 10-m wind speed U_{10} from WRF model (seen in Fig. 1a).

4 The Improved WBL Theory Applied in the UUCM

Section 3 reflects two shortcomings in the current WBL theory applied in the coupled system. Firstly, the spray-induced stress caused by the interaction between spray droplets and airflow has not been taken into consideration. This may lead the model fail to simulate the air-sea momentum flux in high wind conditions. Many studies have demonstrated the spray-induced stress plays an important role in estimation of the momentum flux in the WBL (Innocentini & Gonçalves, 2010; Wu et al., 2015). Secondly, although supposing logarithmic wind profiles makes the calculation process less complexity, it cannot accurately evaluate the wind speed influenced by wind-induced and spray-induced stress in Eq. (8). Therefore, in this section, the improved WBL theory described in section 1 is applied in the coupled model to deal with these two issues one by one.

The spray-induced stress in Eq. (4) is expressed as (Zhao et al., 2006; Zhang et al., 2016),

$$\tau_{sp}(z) = \frac{4\pi}{3}\rho_w exp(-7z/\delta)\int_{r_L}^{r_H} u_{sp}(z) r^3 \frac{dF(\Omega, u_*)}{dr}\ dr\ , \tag{14}$$

where r_L and r_H are limits for the radius of spray droplets; $dF(\Omega, u_*)/dr$ is the sea spray generation function which is related to wave age Ω (the detail is seen in Zhao et al. (2006)); and $\delta = 0.02 \times U_{10}^2$ is the decay function. Here, the mean horizontal velocity of spray droplets $u_{sp}(z)$ is assumed to equal to $U(z)$. Considering the friction velocity u_* in the new WBL theory varies with height, the drag coefficient as a function of $u_*(z)$ is written as

$$C_d(z) = \left(\frac{u_*(z)}{U_{10}}\right)^2 = \left(\frac{u_*(z)}{\int_{z_0}^{10} 1/K\left(\rho_a u_{*h}^2 - \tau_w(z) + \tau_{sp}(z)\right)/\rho\ dz}\right)^2 , \tag{15}$$

where U_{10} is resulted from the wind profile in Eq. (8). In comparison with Eq. (13), the $C_d(z)$ in Eq. (15) is a function of height other than sustaining constant along z axis. Furthermore, the turbulent stress in basis of Eq. (15) is written as

$$\tau_t(z) = \rho u_*^2(z) = \left(\frac{U_{10} u_*(z)}{\int_{z_0}^{10} 1/K \left(\rho_a u_{*h}^2 - \tau_w(z) + \tau_{sp}(z) \right) / \rho \; dz} \right)^2 . \tag{16}$$

The discrepancy in Eq. (12) and Eq. (16) implies the wave-induced and spray-induced stress should be also incorporated into the coupling fields of the models. After the coupled system starting up, the calculation of wave-induced and spray-induced stress computed in the wave model are regularly transported upward to the atmosphere model. Similarly, atmosphere model transports the 10-m wind fields downward to the WW3 as a forcing.

5 One-Dimensional Idealized Simulations

5.1 Model Setting and Experiment Design

To test the performance of the WBL theories on coupled system, one-dimensional (1D) idealized simulates are conducted. For the coupled system, the 1D single column model set by the WRF is adopted with the domain center being located at ocean surface. The whole domain is set on a hypothetical deep ocean with a uniform water depth of 5000 m so that effects of land and shallow water are taken no into account. The coupling fields exchange variables every five minutes, and the simulated results output every three hours. The MYNN-2.5 boundary layer parameterization is adopted in WRF and the radiation, vapor and cloud schemes are turned off. For the WBL module in the coupled system, the turbulent momentum flux is computed through Eq. (12) and Eq. (16) respectively.

To investigate the impact of the traditional and improved WBL theories on the coupled system from low to high winds, 14 experiments are conducted. The simulation time of each experiments is 96 hours, which roughly equals to the period of a tropical cyclones. Seven of these experiments applying the traditional WBL theory are named Exp-TR shown in Table 1. The others applying the improved WBL theory are named Exp-IM also shown in Table 1. With an interval of $20\,\mathrm{m\,s^{-1}}$, the geostrophic winds ranging from $10\,\mathrm{m\,s^{-1}}$ to $130\,\mathrm{m\,s^{-1}}$ are the initial condition for the 1D simulations.

5.2 Results and Analysis

Figure 2 shows the time-averaged drag coefficients versus 10-m wind speeds (i.e., U_{10}) obtained from numerical experiments. The drag coefficients computed from Exp-TRs level off under high wind conditions. However, over the mean sea surface, C_d resulted from Exp-IMs at different heights begins to decrease when U_{10} exceeds $25\,\mathrm{m\,s^{-1}}$. This is inagreement with the fields observations published by Powell et al. (2003) and Jarosz et al. (2007). It's also noted that the simulated C_d increases with height for all wind speeds. That is to say, the turbulent momentum flux at high levels are larger than that at lower places. Such phenomenon indicates the majority of turbulent momentum are transported into the surface waves and ocean spray at lower levels so that the turbulent momentum flux is smaller. In addition, the relations from COARE 3.5 and Kudryavtsev and Makin (2011) are also plotted in Fig. 2. The former (dash-dotted line) is only applicable for low-to-moderate winds since it shows the monotonic growth of C_d with U_{10} at high winds. The latter (dotted line) is consistent with the simulated results of Exp-IMs at 2 m above the mean sea surface.

In order to investigate the relationship between drag coefficients, mean wind fields and wave ages, C_d versus wave wave Ω in different ranges of U_{10} are shown in Fig. 3. The subplots Fig. 3a and Fig. 3b are respectively resulted from Exp-IMs and Exp-TRs. The C_{d6} in Exp-IMs is chosen since its ranges have the same magnitude as those of C_d in Exp-TRs for all wind speeds (shown in Fig. 2). The scatter points linked by one solid lines result from one experiment. As seen in Fig. 3a, the drag coefficient firstly decreases with increasing wave age when U_{10} is larger than $20\,\mathrm{m\,s^{-1}}$. This owns to the generation of ocean spray droplets under high winds. For more developed wave fields, more spray droplets are produced so that more momentum are transferred from the airflow to them. In contrast, the variance between C_d and U_{10} cannot be seen in Fig. 3b. It's also shown in Fig. 3a that the maximum and minimum of wave ages, as well as the ranges of Ω, decrease with increasing wind speed. Such phenomenon suggests young waves dominate the sea surface at high wind conditions, which consists with the conclusion of Moon et al. (2004). However, Fig. 2b cannot simulate this behavior relating the development stages of surface waves and 10-m wind speeds.

In summary, coupled model applied the improved WBL could simulate two physical processes that the traditional one cannot. One is the reduction in drag coefficients with increasing wind speeds at high winds. The other one is the correlation between the development stage of wave fields and 10-m wind speed.

6 Conclusion and Discussion

The WBL theory plays a crucial role on the estimation of air-sea momentum fluxes in oceanic and atmospheric modeling. Surface waves and ocean spray significantly influence the turbulent momentum fluxes in the WBL. Although the assumption on the constant turbulent momentum flux is widely used the numerical models, the simulated results still present a large deviations compared with field observations, especially for high wind conditions. Therefore, it's necessary to propose the WBL applicable for low-to-extreme winds.

The most important innovation of present study is improving the WBL theory applied in the numerical atmosphere-wave coupled model. The improved WBL theory is based on the governing equations of airflow with suspended particles. In this case, the spray impact on momentum fluxes and wind profiles are introduced to the WBL module of the coupled system. In the improved WBL theory, the momentum flux varies with height rather than sustaining constant. What's more, the wind profile affected by surface waves and spray droplets are explicitly computed in the model instead of assuming its shape in advance. Applying the improved WBL theory to the coupled system, the results of a series of one-dimensional simulations reveal three main findings. Firstly, the simulated drag coefficients obtained from the improved WBL theory agree better with the field observations. Particularly, the drag coefficients varying with height could cover the ranges of measurement data from low to high winds. Secondly, the drag coefficients decrease with growing wave ages for 10-m wind speed up to $20\,\mathrm{m\,s^{-1}}$. Thirdly, there is a strong correlation between 10-m wind speeds and wave fields that young surface waves dominate the sea surface under high wind conditions. On the other hand, when the coupled model applies the traditional WBL theory, three findings different from those above are shown. The simulated drag coefficients can only capture the trend of the observations at low-to-moderate winds and depart from the measurements under high winds. The drag coefficient maintain constant regardless of wave ages. There is no significant relationship between 10-m wind speeds and development stages of wave fields.

Although the coupled model with the improved WBL theory could simulate some physical process occurred at high winds and provide possible mechanism interpretation, it's necessary to conduct the real cases, such as three-dimensional tropical cyclones. In addition, the interaction between surface waves and ocean current is also important to estimate the wave-induced stress. The ocean model should be coupled to the current atmosphere-wave coupled model in the further work.

Acknowledgments

Ting Zhang is supported by China Scholarship Council. The datasets for this research are

included in this paper (and its supplementary information files): Banner et al. (1999), Powell et al. (2003), and Jarosz et al. (2007).

References

Andreas, E. L. (2004). Spray stress revisited. *Journal of physical oceanography*, *34*(6), 1429–1440.

Banner, M. L., Chen, W., Walsh, E. J., Jensen, J. B., Lee, S., & Fandry, C. B. (1999). The southern ocean waves experiment. part i: Overview and mean results. *Journal of Physical Oceanography*, *29*(9), 2130–2145.

Barenblatt, G. I. (1953). On the motion of suspended particles in a turbulent flow. *Prikl Mat Mekh*, *17*(1), 261–721.

Donelan, M. A., Haus, B. K., Reul, N., Plant, W. J., Stiassnie, M., Graber, H. C., ... Saltzman, E. S. (2004). On the limiting aerodynamic roughness of the ocean in very strong winds. *Geophysical Research Letters*, *31*(18).

Drennan, W. M., Graber, H. C., Hauser, D., & Quentin, C. (2003). On the wave age dependence of wind stress over pure wind seas. *Journal of Geophysical Research*, *108*(3), 10–11.

Hara, T., & Belcher, S. E. (2004). Wind profile and drag coefficient over mature ocean surface wave spectra. *Journal of physical oceanography*, *34*(11), 2345–2358.

Innocentini, V., & Gonçalves, I. A. (2010). The impact of spume droplets and wave stress parameterizations on simulated near-surface maritime wind and temperature. *Journal of Physical Oceanography*, *40*(6), 1373–1389.

Janssen, P. A. (1991). Quasi-linear theory of wind-wave generation applied to wave forecasting. *Journal of physical oceanography*, *21*(11), 1631–1642.

Jarosz, E., Mitchell, D. A., Wang, D. W., & Teague, W. J. (2007). Bottom-up determination of air-sea momentum exchange under a major tropical cyclone. *Science*, *315*(5819), 1707–1709.

Kudryavtsev, Chapron, B., & Makin, V. K. (2014). Impact of wind waves on the air-sea fluxes: A coupled model. *Journal of Geophysical Research*, *119*(2), 1217–1236.

Kudryavtsev, & Makin, V. K. (2011). Impact of ocean spray on the dynamics of the marine atmospheric boundary layer. *Boundary-Layer Meteorology*, *140*(3), 383–410.

Liu, B., Guan, C., & Xie, L. (2012). The wave state and sea spray related parameterization of wind stress applicable from low to extreme winds. *Journal of Geophysical Research: Oceans*, *117*(C11).

Makin, V., & Kudryavtsev, V. (1999). Coupled sea surface-atmosphere model: 1. wind over waves coupling. *Journal of Geophysical Research: Oceans*, *104*(C4), 7613–7623.

Makin, V., & Mastenbroek, C. (1996). Impact of waves on air-sea exchange of sensible heat and momentum. *Boundary-Layer Meteorology*, *79*(3), 279–300.

Moon, I., Ginis, I., & Hara, T. (2004). Effect of surface waves on charnock coefficient under tropical cyclones. *Geophysical Research Letters*, *31*(20).

Powell, M. D., Vickery, P. J., & Reinhold, T. A. (2003). Reduced drag coefficient for high wind speeds in tropical cyclones. *Nature*, *422*(6929), 279–283.

Stewart, R. (1974). The air-sea momentum exchange. *Boundary-Layer Meteorology*, *6*(1-2), 151–167.

Taylor, P. K., & Yelland, M. J. (2001). The dependence of sea surface roughness on the height and steepness of the waves. *Journal of physical oceanography*, *31*(2), 572–590.

Wu, L., Rutgersson, A., & Nilsson, E. (2017). Atmospheric boundary layer turbulence closure scheme for wind-following swell conditions. *Journal of the Atmospheric Sciences*, *74*(7), 2363–2382.

Wu, L., Rutgersson, A., Sahlee, E., & Larsen, X. G. (2015). The impact of waves and sea spray on modelling storm track and development. *Tellus A*, *67*(1), 27967.

Zhang, T., & Song, J. (2018). Effects of sea-surface waves and ocean spray on air–sea momentum fluxes. *Advances in Atmospheric Sciences*, *35*(4), 469–478.

Zhang, T., Song, J., Li, S., & Yang, L. (2016). The effects of wind-driven waves and ocean spray on the drag coefficient and near-surface wind profiles over the ocean. *Acta Oceanologica Sinica*, *35*(11), 79–85.
Zhao, D., Toba, Y., Sugioka, K., & Komori, S. (2006). New sea spray generation function for spume droplets. *Journal of Geophysical Research*, *111*.
Zweers, N. C., Makin, V. K., De Vries, J., & Kudryavtsev, V. (2015). The impact of spray-mediated enhanced enthalpy and reduced drag coefficients in the modelling of tropical cyclones. *Boundary-Layer Meteorology*, *155*(3), 501–514.

Appendix: The balanced Equations of Mass and Momentum

A rectangular coordinate $(x_1, x_2, x_3) = (x, y, z)$ is adopted here, where x and y are horizontal, and z is vertical upward with $z = 0$ at the mean sea surface. (u_1, u_2, u_3), (u_{1a}, u_{2a}, u_{3a}) and (u_{1s}, u_{2s}, u_{3s}) separately denote velocities of the mixture, airflow and spray droplets along (x, y, z) directions, where the mixture denotes the airflow containing spray droplets.

Postulations (i) and (ii) permit us to assume spray droplets form a continuous distribution in the airflow. Above surface waves, the density of the mixture is written as

$$\rho = \rho_a(1-s) + \rho_w s = \rho_a + (\rho_w - \rho_a)s \ , \tag{1}$$

where s is the volume concentration of spray droplets, ρ_a and ρ_w are densities of the air and water. Defined through the mass-weighted mean of the airflow velocity u_{ia} and spray velocity u_{iw}, the mixture velocity u_i can be written as (i =1,2,3)

$$u_i = u_{ia}\frac{\rho_a(1-s)}{\rho} + u_{is}\frac{\rho_w s}{\rho} = u_{ia} - a\delta_{i3}\frac{\rho_w s}{\rho} \ , \quad (i = 1, 2, 3) \ , \tag{2}$$

where the second equation is coincides with the postulation (iii). The a in Eq. (2) is the mean fall velocity of spray droplets, the direction of which is vertical downward.

The continuity and horizontal momentum equations of the mixture are written as

$$\frac{1}{\rho}\left(\frac{\partial \rho}{\partial t} + u_j\frac{\partial \rho}{\partial x_j}\right) + \frac{\partial u_j}{\partial x_j} = 0 \ , \quad (j = 1, 2, 3) \ , \tag{3}$$

$$\rho\left(\frac{\partial u_i}{\partial t} + u_j\frac{\partial u_i}{\partial x_j}\right) = -\frac{\partial p}{\partial x_i} + \sigma_i, \quad (i = 1, 2;\ j = 1, 2, 3) \ , \tag{4}$$

where σ_i is the viscous stress and p is the total pressure. Considering the impact of surface waves on the dynamic of boundary layer as the postulation (v), the velocities of the mixture, airflow, total pressure and viscous stress could be decomposed as following

$$u_i = \overline{u_i} + \widetilde{u}_i + u_i' \ , \quad (i = 1, 2) \ , \tag{5}$$

$$u_{ia} = \overline{u_{ia}} + \widetilde{u_{ia}} + u_{ia}' \ , \quad (i = 1, 2) \ , \tag{6}$$

$$\sigma_i = \overline{\sigma_i} + \widetilde{\sigma}_i + \sigma' \ , \quad (i = 1, 2) \ , \tag{7}$$

$$p = \overline{p} + \widetilde{p} + p' \ , \quad (i = 1, 2) \ , \tag{8}$$

$$s = \overline{s} + \widetilde{s} + s' \ , \quad (i = 1, 2) \ , \tag{9}$$

where the overbar denotes the time averaging, the wave-tilde denotes the wave-related part and prime denotes the turbulent fluctuation. According to the postulation (i), we obtain $\overline{u_i} = \overline{u_i}(z)$, $\overline{u_i} = \overline{u_i}(z)$, $\overline{\sigma_i} = \overline{\sigma(z)}$ and $\overline{p} = \overline{p}(z)$. Thus, the time averaging equations of the continuity Eq. 3 momentum Eq. 4 for the mixture could be written as

$$\frac{\partial \overline{u_j}}{\partial x_j} = 0 \ , \quad (j = 1, 2, 3) \ , \tag{10}$$

$$\frac{\partial \overline{u_i u_j}}{\partial x_j} = \overline{\sigma_i} \ . \quad (i = 1, 2; \ j = 1, 2, 3) \ , \tag{11}$$

Applying the postulation (iv), Eq. (2) and Eq. (5)-Eq. (10) to Eq. (11), the horizontal momentum equation of the airflow Eq. (11) could be written as

$$\frac{\partial}{\partial x_3}\left(\overline{\widetilde{u_{ia}}\widetilde{u_{3a}}} + \overline{u'_{ia}u'_{3a}} - \overline{\frac{\rho_w}{\rho}u'_{ia}s'a}\right) = 0 \ , \quad (i = 1, 2) \ , \tag{12}$$

where the terms multiplied by $\overline{\widetilde{u_{ia}}u'_{3a}}$, $\overline{\widetilde{u_{3a}}u'_{ia}}$, $\overline{\widetilde{u_{ia}}\widetilde{s}}$, $\overline{\widetilde{u_{ia}}s'}$ and $\overline{u'_{ia}s'}$ are neglected as we regard they are too small compared with other terms. The mean velocity of the airflow is assumed zero here, i.e., $\overline{u_{3a}} = 0$, since vertical motions of the airflow could be neglected compared with its horizontal motions. In addition, the viscous stress $\overline{\sigma_i}$ in Eq. (12) is regarded zero since it only influences the very-near surface layer. The parameterization of this viscous layer is normally adopted instead of the explicit description of the viscous stress (Makin & Kudryavtsev, 1999).

Introducing the mean horizontal velocity $\overline{U}$, wave-induced velocity $\widetilde{U}$ and turbulent-induced velocity U' of the airflow to Eq. (12). Then Eq. (12) could be rewritten as

$$\frac{\partial}{\partial z}\left(\overline{\widetilde{U}\widetilde{w}} + \overline{U'w'} - \overline{\frac{\rho_w}{\rho}U's'a}\right) = 0 \ , \tag{13}$$

where $\overline{U} = \sqrt{(\overline{u_{1a}})^2 + (\overline{u_{2a}})^2}$, $\widetilde{U} = \sqrt{(\widetilde{u_{1a}})^2 + (\widetilde{u_{2a}})^2}$ and $U' = \sqrt{(u'_{1a})^2 + (u'_{2a})^2}$. The $\widetilde{w}$ and w' in Eq. (13) denote the wave-induced and turbulent-induced vertical velocities of the airflow, i.e., $\widetilde{w} = \widetilde{u_{3a}}$ and $w' = u'_{3a}$.

Table 1. Experiment designs

Experiment Design		Experiment Design	
Name of the Experiment	$U_g(\mathrm{m\,s^{-1}})$	Name of the Experiment	$U_g(\mathrm{m\,s^{-1}})$
Exp-TR-1	10	Exp-IM-1	10
Exp-TR-2	30	Exp-IM-2	30
Exp-TR-3	50	Exp-IM-3	50
Exp-TR-4	70	Exp-IM-4	70
Exp-TR-5	90	Exp-IM-5	90
Exp-TR-6	110	Exp-IM-6	110
Exp-TR-7	130	Exp-IM-7	130

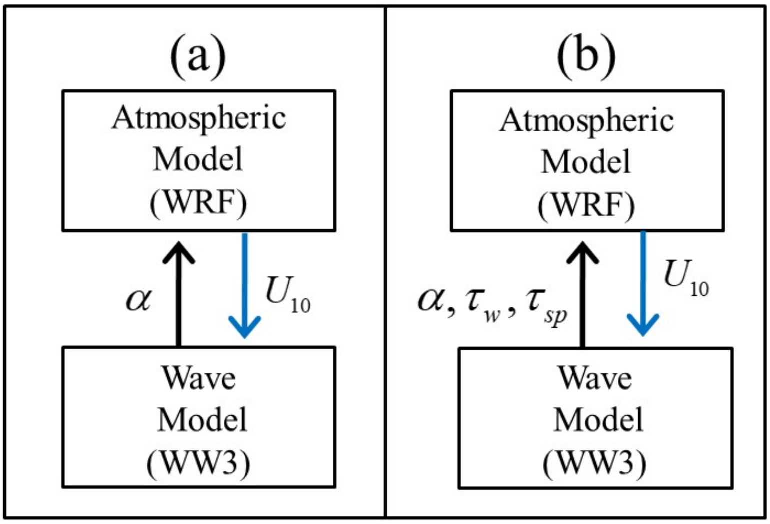

Figure 1. Schematic illustration of the coupled model. Here α is the Charnock coefficient, U_{10} is the 10-m wind speed, $\tau_w(z)$ is the wave-induced stress and $\tau_{sp}(z)$ is the spray-induced stress.

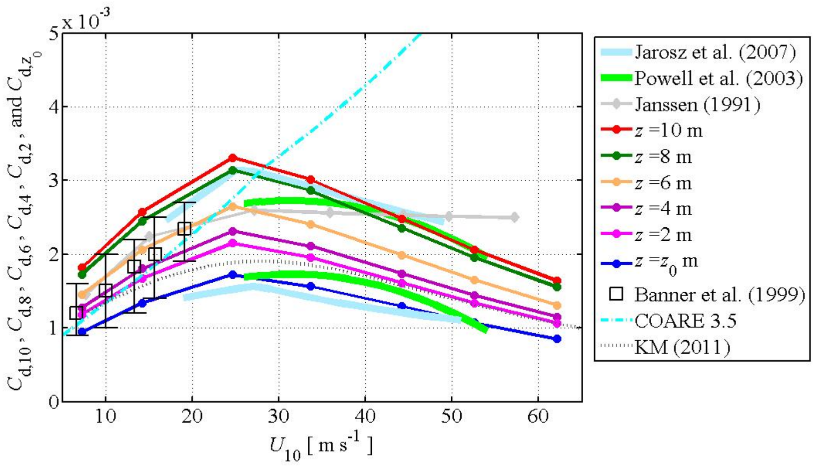

Figure 2. Drag coefficients versus mean 10-m wind speed. Circles represent the results obtained from Exp-IM-1 to Exp-IM-7. Diamonds represent the results obtained from Exp-TR-1 to Exp-TR-7. Blue and green lines are the upper and lower limits of observations from Jarosz et al. (2007) and Powell et al. (2003). Vertical bars of the squares represent the rang of estimation based on 95% limits.

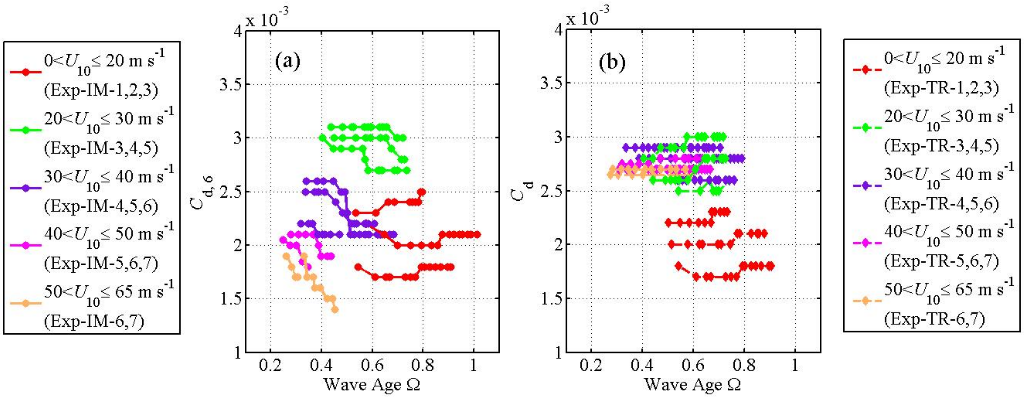

Figure 3. Drag coefficients versus wave age for various ranges of wind speed. Results from Exp-IM (a) and Exp-TR (b).